machines

Article

Experimental Research on the Coupling Relationship between Fishtail Stiffness and Undulatory Frequency

Yuanhao Zhang [1], Rongjie Kang [1,2], Donato Romano [3,4], Paolo Dario [2,3,4] and Zhibin Song [1,2,*]

1 School of Mechanical Engineering, Tianjin University, Tianjin 300354, China; zyh2020@tju.edu.cn (Y.Z.); rjkang@tju.edu.cn (R.K.)
2 Mechanism Theory and Equipment Design of the Ministry of Education, Centre for Advanced Mechanisms and Robotics, Tianjin University, Tianjin 300354, China; paolo.dario@santannapisa.it
3 The BioRobotics Institute, Scuola Superiore Sant'Anna, 56100 Pisa, Italy; donato.romano@santannapisa.it
4 Department of Excellence in Robotics and AI, Scuola Superiore Sant'Anna, 56100 Pisa, Italy
* Correspondence: songzhibin@tju.edu.cn

Abstract: Fish can swim in a variety of states. For example, they look flexible and perform low-frequency undulatory locomotion when cruising, but they seem very powerful and stiff and perform high-frequency undulatory when hunting. In the process of changing the motion state, the stiffness of the fish body affects the swimming performance of the fish. In this article, we imitated the change of stiffness by superimposing rubber sheets and used experimental methods to test its swimming performance under different swing frequencies. A series of rubber fish tails were made according to the analysis of the swimming movement of real fish, providing different stiffness values and changing the curves of the body. In the prototype experiments, the base of the fish tail was fixed to a platform via a force sensor, which can oscillate at various speeds, so that the fish tail was able to swing and the thrust could be tested at different frequencies. According to the experimental results, we found that with the change of the swing frequency, there were different optimal stiffnesses that could make the thrust reach the maximum value, and with the increase of stiffness, the envelope interval of the swing curve gradually widened, the amplitude increased, and the hysteresis of the tail fin relative to the end decreased.

Keywords: rubber sheet; tail stiffness; swing frequency; swing curve

Citation: Zhang, Y.; Kang, R.; Romano, D.; Dario, P.; Song, Z. Experimental Research on the Coupling Relationship between Fishtail Stiffness and Undulatory Frequency. *Machines* **2022**, *10*, 182. https://doi.org/10.3390/machines10030182

Academic Editor: Davide Astolfi

Received: 25 January 2022
Accepted: 22 February 2022
Published: 3 March 2022

1. Introduction

Research on biomimetic fish is mainly based on the body and/or caudal fin (BCF) mode, which produces a high swimming speed, high efficiency, and fast starting performance. With regards to the mechanical structure, it can be divided into series type, parallel type, series parallel type, flexible structure, and so on [1].

The serial multi joint bionic fish is the most representative structure in bionic fish, such as the well-known robot fish tuna at MIT [2] and G9 [3] at Essex University. Although it has relatively excellent performance in all kinds of bionic fish, its performance is still far from that of real fish. The swing curve of the multi joint bionic fish's tail is completely obtained by active control, having no interaction with the surrounding water, which is a large difference between the swimming curve of the bionic fish and that of real fish.

Bionic fish with a flexible structure have also been widely regarded. Its structure is relatively simple, and the flexible tail is driven passively only by the front end. For example, MIT's Valdivia [4] bionic fish made of viscous materials is a typical structure, one that applies sinusoidal excitation in the middle to stimulate the movement of elastic fish tail. The flexible robot fish has a reliable structure, simple control, low cost, and high mechanical efficiency. The tail of the whole flexible material swings passively in the water to simulate the movement of the real fish tail. The passive structure can adapt well to the changes of the water environment. However, once it is completed, the mechanical characteristics of mechanical fish such as stiffness and damping cannot be changed [5], making it unable to perform in a wide range of swing frequencies.

Biomechanical research [6] shows that the skin, tendons, and bone of fish can act as springs to change their own stiffness, so as to better adapt to different swimming conditions. The variable stiffness characteristics of simulated fish can make the robotic fish obtain better swimming performance and behave more like real fish. Therefore, we need to know more about the influence of the stiffness of the fish tail on swimming performance.

In this paper, we designed an experiment to test the passive motion of a large number of fishtails with different stiffnesses under different input conditions. To explore the natural coupling relationship between the different stiffness of the fish body and the oscillation frequency and amplitude, we superimposed ethylene-propylene rubber sheets of different shapes to make fish tails, thereby simulating the changes of fish tail stiffness. One end of the fishtail is fixed on the rotating shaft, which swings by taking the angle of the sine function as input, and its thrust and other properties are measured.

Scholars have proposed multiple ways to alter the stiffness of bionic fish [7–12] and have proposed a variety of methods to achieve variable stiffness, as Table 1 shows. Zuo [7] proposed a planar model of oscillatory propulsor with variable stiffnesses using hyper-redundant serial-parallel mechanisms. Sanaz [8] simulated the fishtail with variable stiffnesses through a multi-layer composite fin with an electro rheological fluid core. Jusufi [9] used bilateral contract to modify axial body stiffness during swimming. Kobayashi [10] used a fin with a variable effective length spring to change the stiffness. Li [11] made mechanisms that could be considered as redundant planar rotational parallel mechanisms with antagonistic flexible elements. Xu [12] proposed a variable stiffness mechanism that is based on negative work. There are also some new skins that follow these variable stiffness properties nicely [13].

Table 1. Some studies on changing the stiffness of robotic fish.

Program	Method
Planar model [7]	Hyper redundant serial-parallel mechanisms
Multi-layer composite fin [8]	Electro rheological fluid core
Fish-inspired physical model [9]	Bilateral contract
Novel propulsion mechanism [10]	Fin with a variable effective length spring
Redundant planar rotational parallel mechanisms [11]	Antagonistic flexible elements
Adjustment mechanism [12]	Negative work for high-efficient propulsion

The above studies all provide different methods for changing the stiffness of the fins. However, these methods of changing the stiffness all need to be implemented in a relatively complicated mechanism or manner, and the shape of the mechanism is difficult to change once completed [14]. For some low-cost robotic fish, if one wants to test the effect of different stiffnesses on swimming characteristics under a certain size and frequency, it is often not desirable to take too complicated testing methods.

In this paper, an experimental method was proposed to simulate the stiffness change of robotic fish by superimposing rubber sheets. This experimental method is simple in structure and easy to obtain in terms of materials, having a lower cost and being a more convenient method to study the effect of stiffness on swimming characteristics at different frequencies. This experimental method can provide reference stiffness data for some complex variable-stiffness robotic fish or flexible robotic fish.

2. Theoretical Analysis

It is not easy to analyze the force of flexible fishtail directly [15]. Therefore, we used a simple model to verify the effect of stiffness on swimming performance and analyzed the action mode of the stiffness effect.

First, a fishtail model of a two-joint connecting rod structure was established, as shown in Figure 1a. When the fish tail swings in the water, it is mainly affected by the differential pressure resistance, which is

$$f = C_d \rho S v^2 \tag{1}$$

where C_d is the drag coefficient, which is related to the material and shape of the object; S is the upstream area; and v is the velocity perpendicular to the upstream area. The lengths of the rods are l_1 and l_2, the angle of rod 1 around x is θ_1, and the angular velocity is ω. The angle of rod 2 around rod 1 is θ_2, and remains unchanged. The forward speed of the fish is v_0.

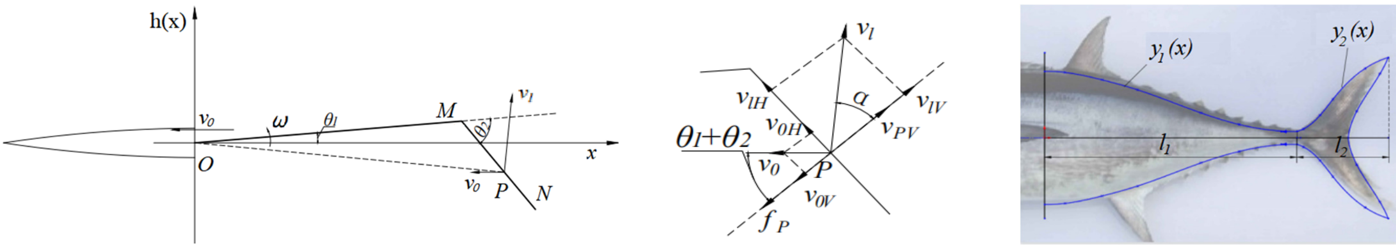

Figure 1. Modeling of fishtail of two-joint connecting rod structure. (**a**) Schematic diagram of two-joint connecting rod structure. (**b**) Forces on a random point on the caudal fin. (**c**) Fitting the profile curve of the fish according to the actual shape of the tuna.

Then the axial thrust on the segment OM is

$$f_1 = -\int_0^{l_1} C_d \rho (\omega x + v_0 \sin\theta_1)^2 \sin\theta_1 y_1(x) dx \tag{2}$$

The stress at any point P on the tail MN section is shown in Figure 1b. Then, the axial thrust of the segment MN is as follows:

$$f_2 = -\int_{l_1}^{l_2} C_d \rho (v_1 \cos\alpha - v_0 \cos(\theta_1 + \theta_2))^2 \sin(\theta_1 + \theta_2) y_2(x) dx \tag{3}$$

$$v_1 = \omega(l_1 + x\cos\theta_2) \tag{4}$$

$$\alpha = \theta_1 + \theta_2 - \arctan\left(\frac{l_1 \sin\theta_1 + l_2 \sin(\theta_1 + \theta_2)}{l_1 \cos\theta_1 + l_2 \cos(\theta_1 + \theta_2)}\right) \tag{5}$$

where C_d is the drag coefficient, and its value is about 0.04 [8], ρ = 1000 kg/m^3. According to the actual shape of the tuna, the side profile curve of tuna is fitted as shown in Figure 1c, and l_1 = 0.3 m, l_2 = 0.1 m, and the shape function of the rubber sheet are as follows:

$$y_1(x) = 12.7x^4 - 1.6x^3 - 1.5x^2 - 0.1x + 0.1 \tag{6}$$

$$y_2(x) = \begin{cases} -781x^4 + 1147x^3 - 643x^2 + 164x - 16 & 0.3 < x \le 0.36 \\ -781x^4 + 1147x^3 - 643x^2 + 164x - 16 - 4.8(x - 0.36) & 0.36 < x \le 0.4 \end{cases} \tag{7}$$

Then, we set v_0 = 0, and input joint θ_1 = π/6sin(2πt); the relationship between axial thrust and rotation angle of the OM section is shown in Figure 2a, and the relationship between axial thrust and rotation angle of the MN section is shown in Figure 2b.

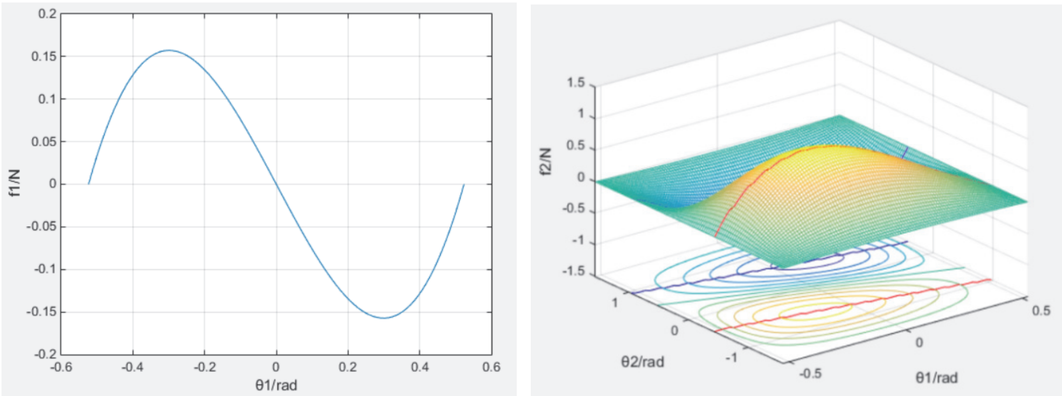

(**a**) (**b**)

Figure 2. Relationship between fishtail thrust and joint angle. (**a**) Fishtail thrust—joint 1 angle. (**b**) Caudal fin thrust—joint 1 rotation and joint 2 rotation.

By comparing the two curves, we found that

(1) The force of MN segment is one order of magnitude higher than that of the OM segment, and in the case of good planning, it shows positive thrust in the whole cycle, that is, the thrust is mainly provided by the caudal fin.

(2) Under different intermediate transmission angles, the change of the tail boom angle has a great influence on the axial thrust. When changing according to the law of the red line, the maximum thrust can be maintained for half a cycle. However, the direction of the fish body swing will change in one cycle. If the maximum thrust θ_2 needs to be changed according to the red line law in the forward swing, it should be changed according to the blue line law in the reverse swing. Moreover, the back-and-forth change θ_2 on the swing boundary must be continuous, and thus the optimal change law of θ_2 and θ_1 is an approximate ellipse.

The above model is sufficient to prove that the caudal fin is the main source of power, and the angle of caudal stalk has a great influence on the forward force. However, there is no joint that can adjust the angle in a real fish, and the trunk is also not a rigid body. The angle of the tail stalk is accumulated by the continuous bending angle of the tail, and its size has a great relationship with the stiffness characteristics of the tail. Under different frequency characteristics, in order to keep the rotation angle within a reasonable range, the stiffness should be changed accordingly. Better adaptation to different frequencies is only possible when the stiffness is further varied.

3. Methods

The purpose of this experiment was to explore the natural coupling relationship between swing frequency, swing amplitude, and stiffness. These include four models with different rates of change in stiffness curves. To ensure the same stress in each experiment, we produced substrates according to the shape of real tuna, as shown in Figure 3.

Figure 3. A thin rubber tail made from the shape of a real tuna.

To design the overlay more reasonably, we first analyzed a tuna swimming video [16]. The bending stiffness was calculated according to the bending stiffness formula as follows:

$$EI = \frac{J\ddot{\theta}}{\psi} \quad (8)$$

where EI is the bending stiffness, J is the moment of inertia, $\ddot{\theta}$ is the angular acceleration, and ψ is the corner. To obtain the stiffness of the middle of the tuna, we should know its moment of inertia, angular acceleration, and curvature. We set the middle part of the fish to the tail handle as an ellipse with a length of 14 cm, a width of 8 cm, a cone with a height of 28 cm, a density of 1000 kg/m^3, and the moment of inertia J = 0.00823375 kgm^2. To calculate the angular acceleration and curvature, we recorded the angle between the middle part of the fish and the head in the video θ. The change of chord length l is recorded in video. The angular acceleration time curve was obtained, and the middle part of the cut was regarded as an arc according to r = l/2sinθ. The curvature time curve was then obtained. We replaced the result back to Equation (6) to obtain the stiffness time curve of the middle part, as shown in Figure 4a. The bending stiffness EI of the middle part of the fish was about 0.08 Nm^2, and its shape was still calculated according to the above assumption, and the approximate stiffness curve of the whole fish tail was obtained (Figure 4b).

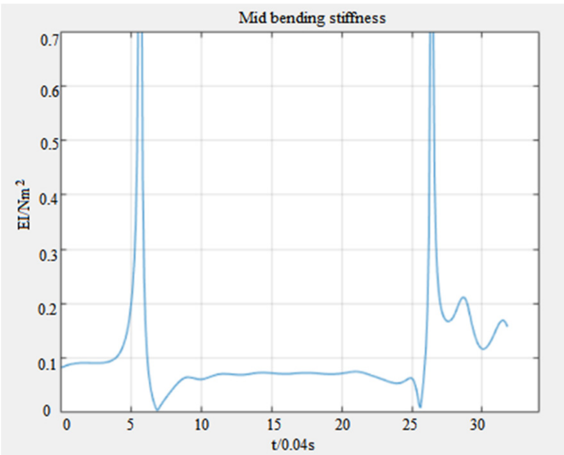

(**a**)

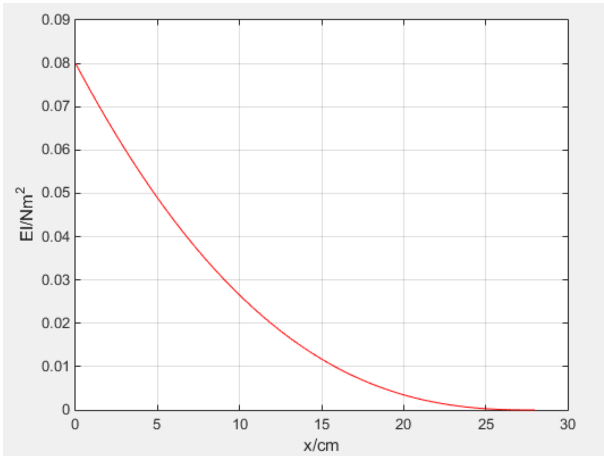

(**b**)

Figure 4. The bending stiffness of tuna tail. (**a**) Stiffness—time curve of fish tail end. (**b**) Calculated stiffness curve of fish tail.

On this basis, we designed the superposition sheet of $y = (7 - 0.25x)^4/343$, $y = (7 - 0.25x)^3/49$, $y = (7 - 0.25x)^2/7$, and $y = (7 - 0.25x)$—four functional curves (Figure 5). Through the superposition of each rubber sheet, we were able to realize four groups of fishtail stiffness curves. For easy identification, we used end stiffness values to represent the stiffness of a particular stiffness curve, such as that shown in Figure 5d, whose stiffness was recorded as 0.28672.

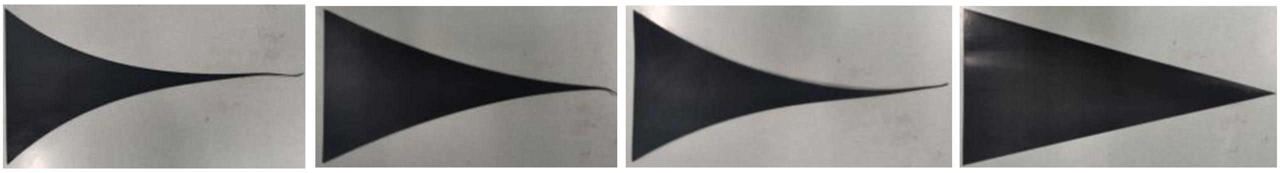

(**a**) (**b**) (**c**) (**d**)

Figure 5. Four kinds of fishtail flakes with different stiffness change rates. (**a**) Rubber tail slice cut according to the curve $y = (7 - 0.25x)^4/343$. (**b**) Rubber tail slice cut according to the curve $y = (7 - 0.25x)^3/49$. (**c**) Rubber tail slice cut according to the curve $y = (7 - 0.25x)^2/7$. (**d**) Rubber tail slice cut according to the curve $y = (7 - 0.25x)$.

To quantitatively show the effect of different stiffnesses, we connected the fishtail to the connecting rod, and the whole device was connected to the force sensor, so as to measure its axial force and transverse force (Figure 6a) and make it swing with a sinusoidal change of angle driven by the motor (Figure 6b). In addition, we recorded the voltage and current of the motor to calculate the power under different conditions, so as to judge the swimming efficiency under different conditions.

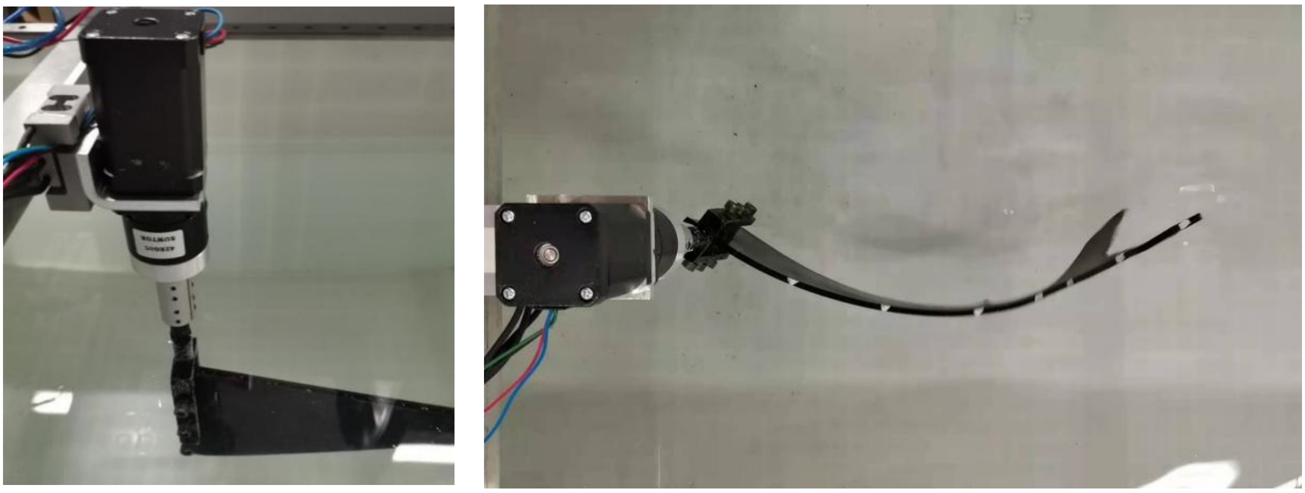

(**a**) (**b**)

Figure 6. Experimental device. (**a**) One end of the fishtail was connected to the connecting rod, which was driven by the motor and connected with the force sensor. (**b**) The fish tail rotated with the connecting rod.

4. Results

First, a rubber substrate with a full fishtail profile was tested. We changed the frequency of the fish tail swing and tested the thrust provided by the fish tail swing separately. After measuring one set of frequencies, we added another piece of rubber on the rubber plate; repeated the experiment above; and obtained the relationship diagram of thrust, frequency, and bending stiffness (Figure 7a).

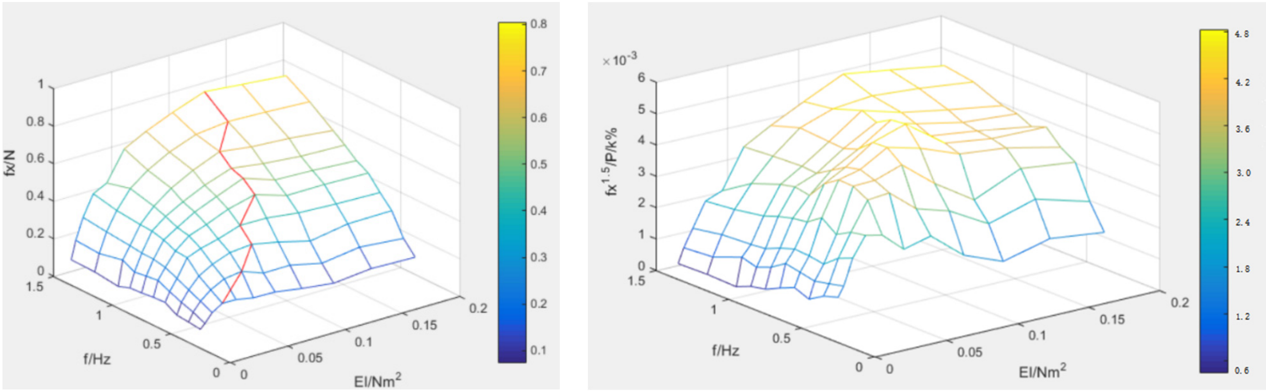

(**a**) (**b**)

Figure 7. Coupling relationship between the stiffness and the swing frequency. (**a**) Thrust—frequency—bending stiffness diagram. The red line represents the bending stiffness at the highest thrust at different frequencies in the measured data. (**b**) Propulsion efficiency—frequency—bending stiffness diagram.

Moreover, the mechanical efficiency of swimming is expressed as follows:

$$\eta = \frac{P_x}{P_\Sigma} = \frac{f_x v_x}{P_\Sigma} \tag{9}$$

where P_x is the power in the forward direction; $P_\sum$ is the total power, expressed by the product of motor voltage and current; f_x is the thrust; and v_x is the forward speed. During the experiment, the end of the fish tail was fixed, being equivalent to the mechanical resistance applied at the end to balance the thrust. In the actual swimming process, the resistance was expressed by the differential pressure resistance of Equation (1), $f_x \propto {v_x}^2$, and it can be expressed as follows:

$$v_x = k\sqrt{f_x} \tag{10}$$

where k is a constant. In addition, the propulsion efficiency can be expressed as follows:

$$\eta = \frac{k f_x^{1.5}}{P_\Sigma} \tag{11}$$

Taking k% as the unit to qualitatively express the propulsion efficiency, we obtained Figure 7b.

In this experiment, the fishtail with the shape curve of $y = (7 - 0.25x)^2$ was tested, and the swing range was $\pm 36°$. The Figure 8 shows the axial force under different coupling conditions of stiffness and oscillation frequency. The red line is the line connecting the stiffness points at the maximum thrust at a certain frequency. As can be seen from the figure:

(1) At each frequency, there was a most appropriate stiffness value to maximize the axial thrust, and at low frequency, with the increase of frequency, the corresponding optimal stiffness value changed faster. In other words, to make the robot fish swim at different frequencies, we needed to adjust the stiffness of the tail to obtain the maximum thrust at each frequency, and the thrust was more sensitive to the stiffness at low frequencies, but less sensitive to the stiffness at high frequencies.

(2) Under a certain fixed stiffness, the thrust increased with the increase of frequency, but the effect of increasing frequency on thrust was more obvious under high stiffness, and the benefit of increasing frequency on thrust was very small under low stiffness, even with negative gain on thrust.

(3) When the stiffness was very low (EI < 0.015 Nm), the thrust increased substantially with increasing stiffnesses, suggesting that the tail is too soft to simulate fish swimming when EI < 0.015 Nm.

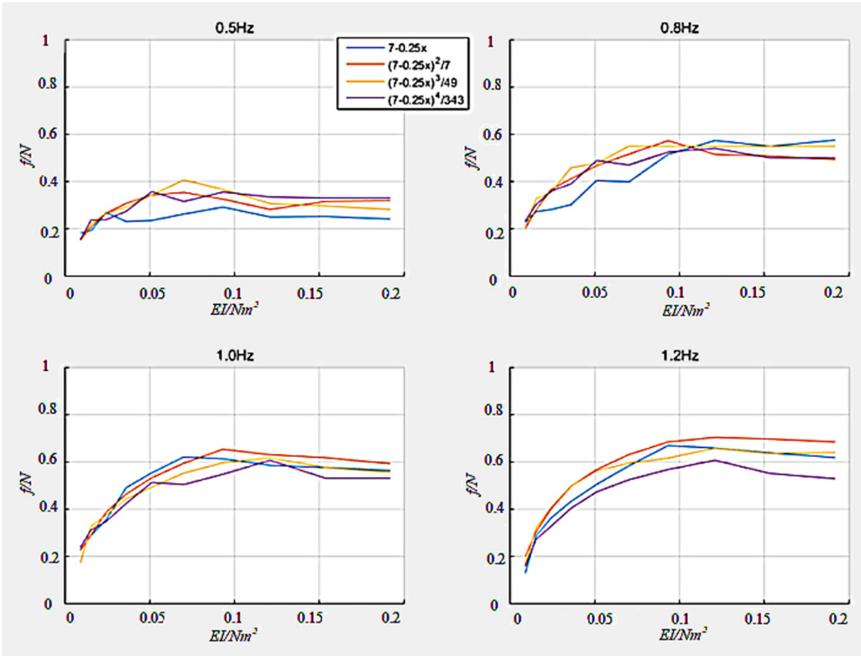

Figure 8. Thrust—bending stiffness diagrams of fish tails with four different rates of change curves under different stiffnesses and frequencies.

The trend of propulsion efficiency was similar to that of the thrust–frequency–stiffness diagram. At the same frequency, when the stiffness made the thrust reach the maximum, the propulsion efficiency was close to the maximum.

It can be seen in Figure 8 that there was little difference in the axial thrust of the fishtail with different stiffness change rates. The fishtail thrust of the second- and third-order functions was slightly higher than that of the first- and fourth-order functions, and thus the stiffness value at which the thrust reached its peak value was found to lag with the increase of the stiffness change rate. The fishtail of the quartic function performed better at low frequencies and had relatively low thrust at high frequencies. The fishtail of the first-order function performed better at high frequencies and lower thrust performed better at low frequencies.

Regardless of the frequency, as the stiffness increased, the envelope of the rocking curve became wider and the amplitude increased. Other things being equal, a high amplitude means a greater relative velocity to the water, which will generate a greater force. At the same time, the curvature of the fishtail curve decreased with increasing stiffness. For the front part of the fishtail, at high curvatures, the attitude that provides thrust took up a higher proportion of a cycle, while at low curvatures, more time in a cycle is to provide drag, which results in a lower thrust-to-drag ratio. For the caudal fin, according to the previous theoretical analysis, the swing angle of the caudal fin will greatly affect the thrust, and at each frequency, with the increase of stiffness, the included angle gradually increased, which also shows that the increase of stiffness will have a greater impact on thrust influence. Furthermore, the degree of hysteresis of the caudal fin relative to the tip decreased as stiffness increased. As shown in Figure 9a, at 0.5 Hz, the caudal fin lagged at about 1/3 cycle, while in Figure 9d, it lagged at about 1/6 cycle.

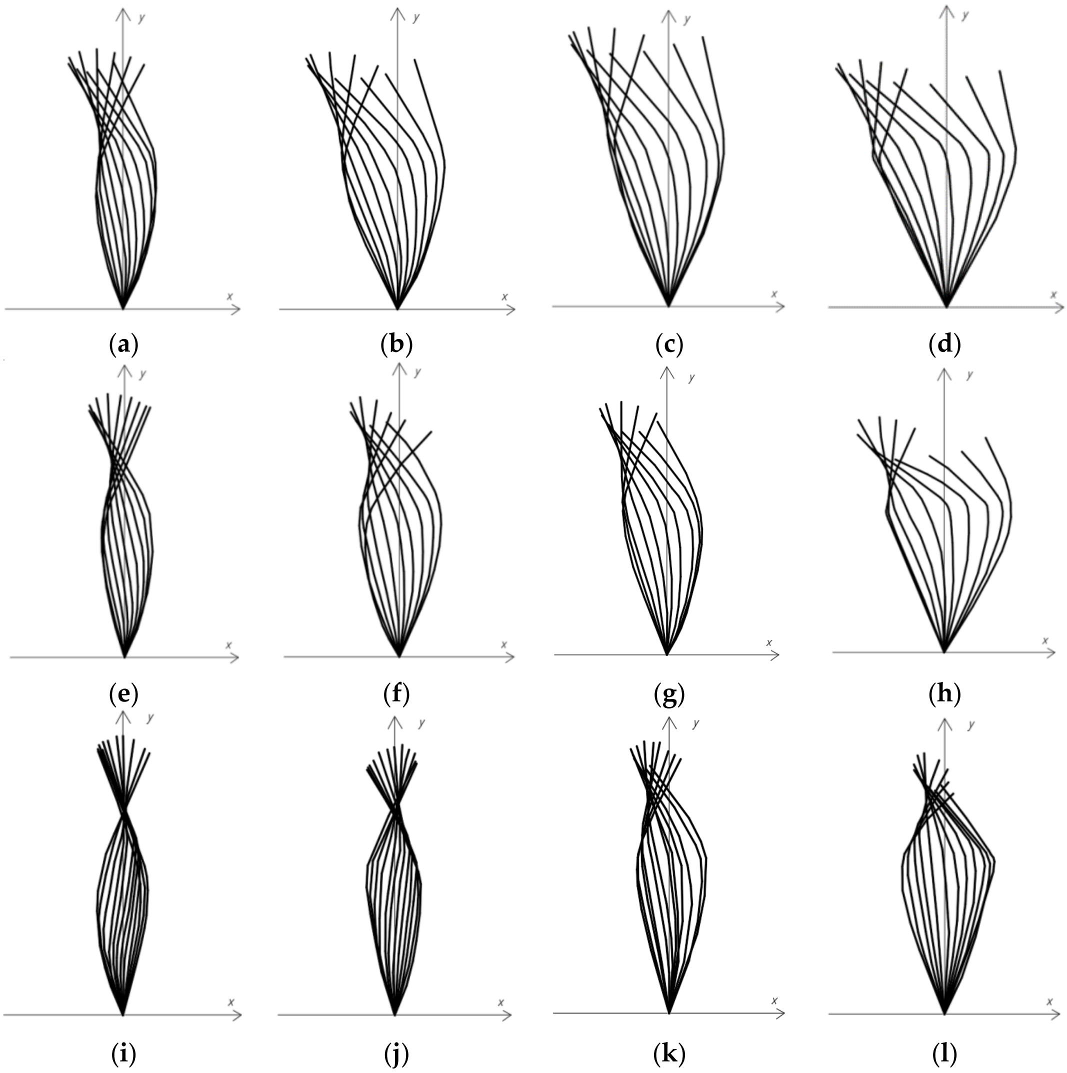

Figure 9. The swing curves of fishtails with different stiffnesses in half cycle at 0.5 Hz, 0.8 Hz, and 1.2 Hz. Each picture depicts the posture of the fish's tail swinging in a half cycle frame by frame in a rectangular coordinate system. Among them, (**a**–**d**) corresponds to four kinds of gradually increasing stiffnesses at 0.8 Hz, (**e**–**h**) corresponds to four kinds of gradually increasing stiffnesses at 0.5 Hz, and (**i**–**l**) corresponds to four kinds of gradually increasing stiffnesses at 1.2 Hz.

In the transverse direction, the amplitude increased with the increase of stiffness, while in the longitudinal direction, the amplitude decreased with the increase of frequency. It can be seen that the swing curve of the high-stiffness fishtail was close to a straight line at low frequencies, as shown in Figure 9d. On the other hand, the fishtail with low stiffness was disordered at high frequency, as shown in Figure 9i,j, wherein the amplitude of the fish tail was very small at this time, and the opposite end of the caudal fin lagged by about half a cycle.

It can be seen in Figure 10 that with the increase of the rate of change of the fishtail stiffnesses, the amplitude of the fishtail swing decreased, and the bending curvature of the fish tail increased. For the triangular curved fishtail, the swing period was closer to a straight line, while for the fourth degree curved fishtail, the degree of curvature was higher during the swing. For the $y = 7 - 0.25x$ curve-shaped fish tail, the caudal fin deflection angle was smaller, and the lag period at the opposite end was reduced. For the fish tail with high-order curve shape, the deflection angle of the tail fin was large, and at high swing frequency, it lagged half a cycle relative to the end, and the swing posture was messy. In addition, with the increase of the swing frequency, the swing amplitudes of the fishtails of the four shapes all decreased.

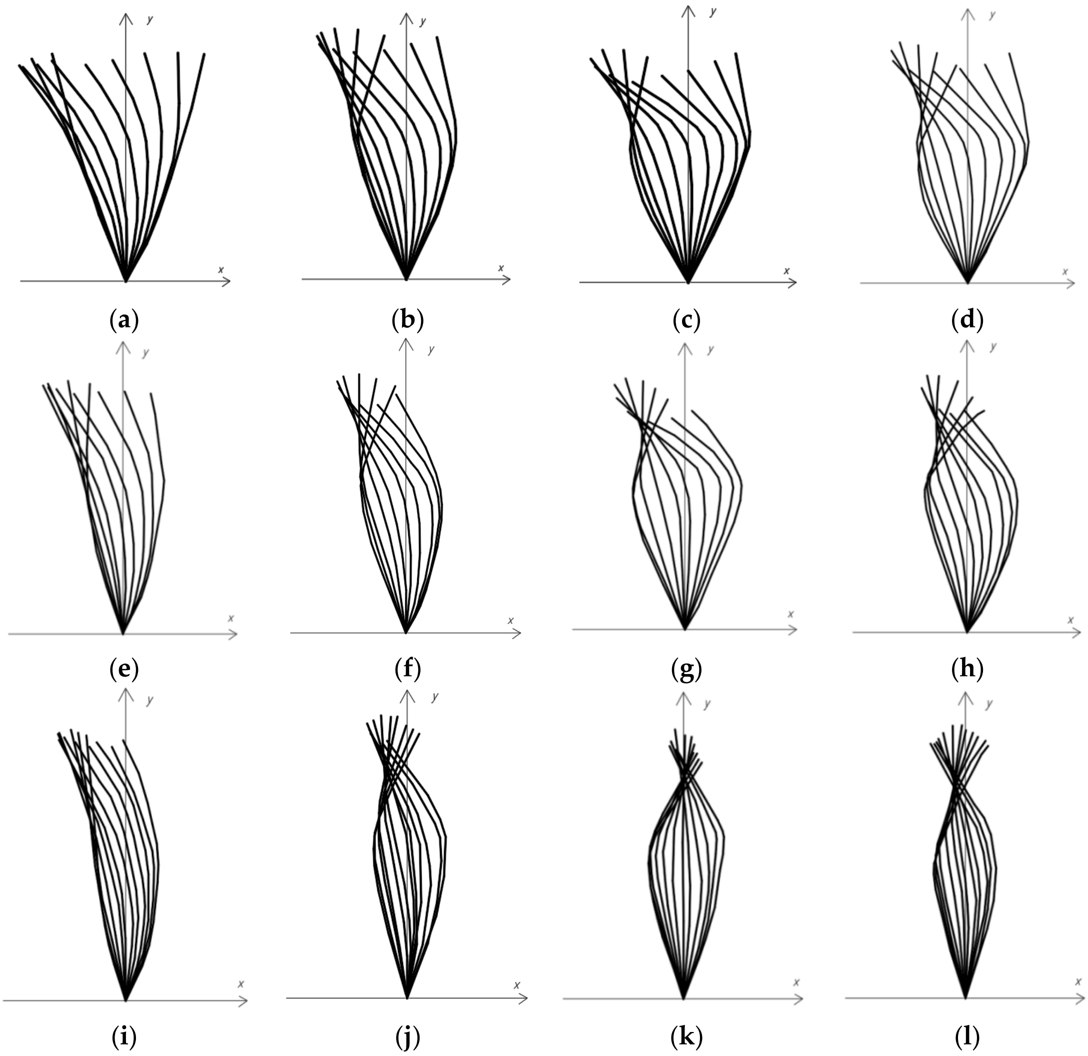

Figure 10. Under the conditions of 0.5 Hz, 0.8 Hz, and 1.2 Hz, we found that the curve of different conversion rates was the same as the curve of fish tail end stiffnesses of 0.03584. From left to right, there were the 1 degree function line, 2 degree function line, 3 degree function line, and 4 degree function line. (**a**–**d**) 0.5 Hz; (**e**–**h**) 0.8 Hz; (**i**–**l**) 1.2 Hz.

5. Conclusions

In this paper, an experimental method of superposition of rubber sheets was proposed to simulate the change of fish stiffness. This method is low-cost, is easy to operate, and can simulate the stiffness characteristics of various forms of bionic fish and obtain the swimming characteristics at this time through a simple swing experiment. In theory, when the stack is subdivided enough, a continuous change in stiffness can be simulated. Through the experiment that the rotating shaft drives the rubber sheet fish tail to swing, the coupling relationship between various fish tail stiffness, shape, and swing frequency can be tested. Moreover, through experiments, we found that with the change of the swing frequency, there were different optimal stiffnesses to make the thrust reach the maximum value, and the lower the frequency, the more sensitive to the change of stiffness. For fish with a tail length of about 0.4 m, the stiffness of the front end of the tail should be in the range of 0.05 to 0.15 Nm^2. The variation trend of propulsion efficiency with frequency stiffness was essentially consistent with the variation trend of thrust with frequency stiffness. It can be seen from the swing curve that with the increase of stiffness, the envelope interval of the swing curve gradually widened, the amplitude increased, and the hysteresis of the tail fin relative to the end decreased. In addition, peak stiffness lagged with an increasing rate of stiffness change, and amplitude decreased with an increasing rate of stiffness change.

Author Contributions: Y.Z. designed the experiment, wrote the manuscript, and analyzed the proposed method. R.K. suggested improvements. D.R. suggested improvements. P.D. suggested improvements. Z.S. is the main author of this paper. He proposed the main idea and plan. All authors have read and agreed to the published version of the manuscript.

Funding: This work was supported by the National Natural Science Foundation of China (NSFC) through grant numbers 51975401 and 51875393 from the major consulting project of academy-local cooperation of the Chinese Academy of Engineering (2021DFZD2).

Institutional Review Board Statement: Not applicable.

Informed Consent Statement: Not applicable.

Data Availability Statement: The data used in this study are openly available in the public domain.

Conflicts of Interest: The authors declare no conflict of interest.

References

1. Yu, J.Z.; Chen, E.K.; Wang, S.; Tan, M. Research evolution and analysis of biomimetic robot fish. *Control. Theory Appl.* **2003**, *20*, 485–491.
2. Anderson, J.M.; Kerrebrock, P.A. The vorticity control unmanned undersea vehicle (VCUUV): An autonomous robot tuna. In Proceedings of the 11th International Symposium on Unmanned Untethered Submersible Technology, Durham, NC, USA, 23–25 September 1999; pp. 63–70.
3. Liu, J.; Dukes, I.; Hu, H. Novel Mechatronics Design for a Robotic Fish. In Proceedings of the IEEE/RSJ International Conference on Intelligent Robots and Systems, Edmonton, AB, Canada, 2–6 August 2005; pp. 2077–2082.
4. Valdivia, P.V. *Design of Biomimetic Compliant Devices for Locomotion in Liquid Environments*; MIT: Midsize City, MA, USA, 2007.
5. Long, J.; Hale, M.; Mchenry, M.; Westneat, M. Functions of fish skin: Flexural stiffness and steady swimming of longnose gar, Lepisosteus osseus. *J. Exp. Biol.* **1996**, *199*, 2139–2151. [CrossRef] [PubMed]
6. Pabst, D.A. Springs in swimming animals. *Am. Zool.* **1996**, *36*, 723–735. [CrossRef]
7. Zuo, C.; Jiang, H.Z. A Study of the Planar Serial-Parallel Mechanism with Various Stiffness for a Biotic Compliant Fish. In *ASME International Mechanical Engineering Congress & Exposition*; American Society of Mechanical Engineers: New York, NY, USA, 2013.
8. Behbahani, S.B.; Tan, X. Design and dynamic modeling of electrorheological fluid-based variable-stiffness fin for robotic fish. *Smart Mater. Struct.* **2017**, *26*, 085014. [CrossRef]
9. Jusufi, A.; Vogt, D.M.; Wood, R.J.; Lauder, G.V. Undulatory Swimming Performance and Body Stiffness Modulation in a Soft Robotic Fish-Inspired Physical Model. *Soft Robot.* **2017**, *4*, 202–210. [CrossRef] [PubMed]
10. Nakabayashi, M.; Kobayashi, R.; Kobayashi, S.; Morikawa, H. A Novel Propulsion Mechanism Using a Fin with a Variable-Effective-Length Spring. In Proceedings of the 2008 IEEE International Conference on Robotics and Biomimetics, Washington, DC, USA, 22–25 February 2009.
11. Li, K.K.; Jiang, H.Z.; Wang, S.Y.; Yu, J.M. A Soft Robotic Fish with Variable-stiffness Decoupled Mechanisms. *J. Bionic Eng.* **2018**, *15*, 599–609. [CrossRef]
12. Xu, D.; Zeng, H.N.; Peng, X.; Zhao, Z.Q.; Liu, J.M. A Stiffness Adjustment Mechanism Based on Negative Work for High-efficient Propulsion of Robotic Fish. *J. Cit. Rep.* **2018**, *15*, 270–282. [CrossRef]
13. Song, Z.B.; Fu, Z.R.; Donato, R.; Paolo, D.; Dai, J.S. A Novel Biomimetic Compliant Structural Skin Based on Composite Materials for Biorobotics Applications. *Soft Robot.* **2021**. [CrossRef] [PubMed]
14. Cheng, J.Y.; Zhuang, L.X.; Tong, B.G. Analysis of swimming 3-D waving plate. *Fluid Mech.* **1991**, *232*, 341–355. [CrossRef]
15. Lighthill, M.J. Large-Amplitude Elongated-Body Theory of Fish Locomotion. *Proc. R. Soc. Lond.* **1971**, *179*, 125–138.
16. Zhu, J.; White, C.; Wainwright, D.K.; Di Santo, V.; Lauder, G.V.; Bart-Smith, H. Tuna robotics: A high-frequency experimental platform exploring the performance space of swimming fishes. *Sci. Robot.* **2019**, *4*, eaax4615. [CrossRef] [PubMed]